

# Coherent Optical Beam Forming with Passive Millimeter-Wave Arrays

P. M. Blanchard, A. H. Greenaway, A. R. Harvey, and K. Webster

**Abstract**—Passive millimeter-wave imaging requires large apertures to achieve an angular resolution comparable to that of typical infrared imagers. Aperture synthesis offers a route to achieving high resolution without using a single large aperture, by interferometrically combining the signals from a number of smaller distributed apertures. In such a system the individual millimeter-wave signals must be transported to a common location with good phase fidelity and combined to form the image. This paper discusses a technique called coherent optical beam forming which performs optical transport of the up-converted millimeter-wave signal and direct image formation at the optical frequency. Proof of principle experiments are described that demonstrate coherent optical beam forming with a point source and a method of self-calibrating the array to remove phase errors.

**Index Terms**—Aperture antennas, array signal processing, millimeter-wave antenna arrays millimeter wave imaging, optical fiber applications, optical image processing optical modulation, phase measurement.

## I. INTRODUCTION

**P**ASSIVE imaging at millimetric wavelengths is attractive due to the improved transmission through fog, cloud and rain in this waveband compared to infrared or visible wavelengths. Passive millimeter-wave images exhibit high contrast between ambient temperature natural background and low temperature sky reflections, and hence look similar to visible images with the same spatial resolution, allowing easy interpretation. High-quality images have been produced using single-scanning dish systems [1], [2], however, due to the relatively long wavelength used (typically 3 or 8 mm) such systems suffer from poor angular resolution compared, for example, to typical infra-red imagers. In order to achieve an angular resolution comparable to a current infra-red imager, a millimeter wave instrument operating at 94 GHz would require a dish diameter greater than 10 m. Instruments of this size made using a single aperture would be extremely heavy, bulky and immobile.

The only practical approaches to achieving significantly higher angular resolution are to use shorter wavelengths (which compromises the all-weather performance) or to synthesize a large aperture by combining the outputs from an array of smaller distributed antennas. Such a sparse array can be used to synthesise an image with the resolution

determined by the maximum separation of antennas rather than the individual antenna size. Each pair of antennas (or baseline) in the array defines a spatial frequency at which the mutual coherence function of the source is measured. An image of the source can be synthesised by Fourier transforming this data [3]. In order to measure the mutual coherence function the signals from each antenna, which may be several meters apart, must be transported to a common location and then combined interferometrically. In order to produce a high-quality image the phase of the signals must be preserved throughout, with an accuracy equivalent to less than about one tenth of a wavelength, leading to a requirement for real-time phase control.

The high attenuation of millimeter-wave transmission lines means that the received signals from an aperture synthesis array must be converted to a more suitable frequency prior to transportation. One possibility is down-conversion to an intermediate frequency (IF) of several GHz, followed by transport along coaxial cables. An alternative is to up-convert either the RF or IF frequency onto an optical carrier frequency and to use optical fibers for transport. By comparison with coaxial cable, optical-fiber has a huge bandwidth, low cost, low attenuation, immunity to electromagnetic (EM) interference and the fractional bandwidth used by the microwave signal is so small that propagation dispersion is negligible. A further advantage is that once the millimeter-wave signals exist on an optical carrier, optical signal processing may be used to manipulate the signals or even generate the image. Economic optical transmission of millimeter-wave signals for aperture synthesis has been made feasible by the widespread adoption of electrooptical transmission in telecommunications. Optical modulators with bandwidths of a few GHz are now readily available and bandwidths of 50 GHz are available at a cost.

The majority of previous work involving the use of optics in array-based RF instruments has been in active rather than passive systems, particularly in the field of phased array radar for both transmitted and received signals [4]. Optical techniques have been proposed and demonstrated for signal transport, signal processing [5], antenna phase and amplitude control, local oscillator distribution, generation of the RF signal by laser interference [6], beam steering and shaping [7]–[9] and implementation of true time delays [10]–[13].

Optical techniques are less developed for passive millimeter-wave imaging applications but have been reported in radio astronomy where optical fibers have been used to carry IF data, LO reference signals, and timing signals [14]. Only

Manuscript received January 5, 1998; revised November 10, 1998.

P. M. Blanchard, A. H. Greenaway, and A. R. Harvey are with the Defence Evaluation and Research Agency, Electronics Sector, Malvern, Worcs, WR14 3PS U.K.

K. Webster is with Sea Sector, Hants, PO17 6AD U.K.

Publisher Item Identifier S 0733-8724(99)01896-4.

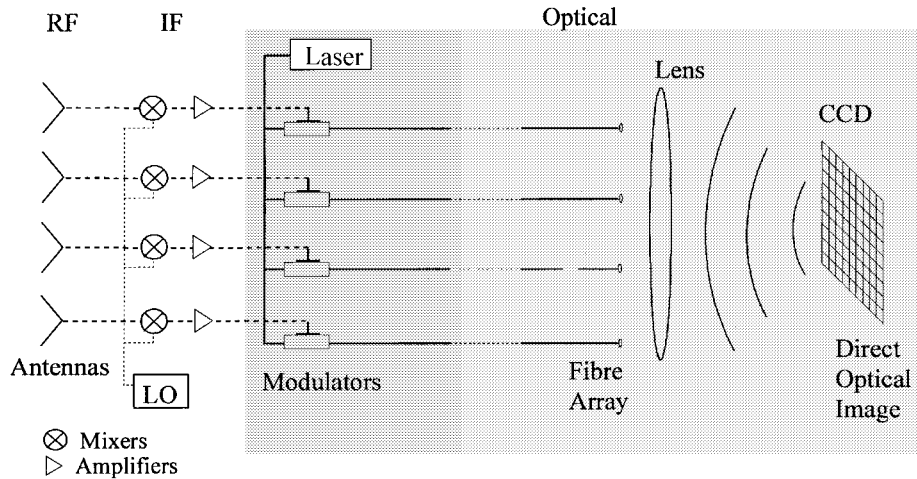


Fig. 1. A schematic diagram of the coherent optical beam-forming technique.

one example of a passive millimeter-wave imaging system that uses optical signal processing and image formation has been developed and demonstrated [15]. The system performs aperture synthesis in one dimension with a linear array of frequency scanned antennas, using the frequency scan to generate the image in the orthogonal direction. A multichannel Bragg cell modulates a laser beam with the millimeter-wave signals and the image is measured directly at the optical wavelength using a charged-coupled device (CCD). The use of bulk-optic Bragg cells and frequency scanned antennas limits the bandwidth and sensitivity of the system.

This paper describes a technique, called coherent optical beam forming, for use with a passive millimeter-wave array-based instrument in which aperture synthesis is performed in two-dimensions and a direct optical image is formed on a CCD. The technique has potential for wider bandwidth operation and approximately an order of magnitude gain in sensitivity compared to frequency scanned approaches. Section II describes the image formation process and the image characteristics in order to allow a deeper understanding of the experimental results described in Section III. During the experiments it was necessary to apply real-time phase control of the optical path lengths, and the approach used (Redundant Spacings Calibration) is described in detail.

## II. COHERENT OPTICAL BEAMFORMING

### A. Basic Concept

Two distinct approaches can be taken to image formation from an array-based instrument. One approach is to take the signal from each antenna, combine it with the signal from every other antenna and use complex correlators to measure the mutual coherence function over each baseline in the array. The image is then generated by calculating the Fourier transform of the data in software. Implementing this approach with an array containing  $N$  antennas requires the signal from each antenna to be divided  $N - 1$  ways, and  $N(N - 1)/2$  complex correlators are needed. Such a system quickly becomes very complex as the number of antennas increases. The alternative is to sum the complex

amplitudes from each antenna prior to detection, which can be conveniently achieved using a lens, with an array detector to measure the image directly. In this case the correlations and Fourier transform are effectively performed by the square-law detector and imaging system, respectively. This approach could be used directly at millimeter-wavelengths but would lead to a large focal plane and a requirement for a millimeter-wave array detector. The concept is much more attractive if the millimeter-wave radiation is converted to optical frequencies prior to image formation, as described here.

The basic components of the coherent optical beam-forming technique, are illustrated in Fig. 1. The millimeter-wave radiation is collected by the antenna array and an electrooptic modulator is used to phase- or amplitude-modulate a laser beam. Depending on the choice of operating wavelength, the noise performance of amplifiers and the bandwidth of modulators available the RF signals may be down-converted to an IF of 1–10 GHz prior to optical modulation. For this down-conversion the LO signal at each antenna must be mutually coherent, but need not necessarily be cophased. The optical signals encoded with the RF phase from each antenna then travel through optical fibers to a central location where image formation occurs. The fiber ends are formed into a two-dimensional (2-D) array that is a scaled version of the RF array and light emerging from the fibers passes through a lens and forms an image of the scene on a CCD camera. The image is formed through interference between the optical beams (encoded with the RF phase), hence all of the optical channels must be mutually coherent. This can be achieved most easily by supplying light from a single laser to each antenna, using fibers for the distribution.

The coherent optical beam-forming technique has several advantages including.

- 1) The maximum baseline of the antenna array is not restricted by transmission losses as it would be if signals were transported through RF waveguide.
- 2) No complex beam-forming system is required. Only one modulator and fiber is required for each antenna and the signals do not have to be split  $N - 1$  ways as in the direct correlation measurement approach.

- 3) A real-time image is generated on the camera.
- 4) Array detectors at visible wavelengths are readily available.
- 5) The imaging optics can be small and remote.

The reduction in complexity of the proposed system compared to the direct correlation measurement technique also has cost implications. An aperture synthesis array containing 100 antennas, would require approximately 5000 complex correlators for the direct measurement approach, whereas only 100 optical modulators would be needed in the optical beam-forming system. The optical technique is likely to be the cheapest solution at today's prices and as the modulator cost is driven down by the telecommunications industry this cost advantage is likely to increase.

### B. Image Formation

In order to produce high-quality images millimeter-wave imagers will require many antenna channels, however for simplicity we will initially consider just two channels. Although the following analysis is written as if the millimeter-wave RF signal is used to modulate the laser, the conclusions would be the same if the RF signal were down-converted to an IF prior to modulation.

The key parameter in determining the ability of the system to form an image is its ability to preserve the phase difference of the RF signal between individual antennas. It is this phase difference, the phase of the mutual coherence function at the spatial frequency sampled by the baseline, that carries the image information and must be transferred to the optical domain. Consider two channels detecting RF signals with phases of  $\phi^a$  and  $\phi^b$ , respectively, giving a baseline phase difference of  $\Delta\phi_{\text{RF}} = \phi^b - \phi^a$ . For amplitude modulation of an optical carrier of angular frequency  $\omega_{\text{opt}}$  by a RF signal of angular frequency  $\omega_{\text{RF}}$  the  $E$ -fields of the optical signals from the two antennas are given by

$$\begin{aligned}
 E^a &= |E^a| \alpha \cdot [1 + \beta \cos(\omega_{\text{RF}}t + \phi^a)] \cdot \cos(\omega_{\text{opt}}t + \phi_{\text{opt}}^a) \\
 &= |E^a| \alpha \cdot \left[ \cos(\omega_{\text{opt}}t + \phi_{\text{opt}}^a) + \frac{\beta}{2} \cos[(\omega_{\text{opt}} + \omega_{\text{RF}})t \right. \\
 &\quad \left. + \phi_{\text{opt}}^a + \phi^a] + \frac{\beta}{2} \cos[(\omega_{\text{opt}} - \omega_{\text{RF}})t + \phi_{\text{opt}}^a - \phi^a] \right] \\
 E^b &= |E^b| \alpha \cdot \left[ \cos(\omega_{\text{opt}}t + \phi_{\text{opt}}^b) + \frac{\beta}{2} \cos[(\omega_{\text{opt}} + \omega_{\text{RF}})t \right. \\
 &\quad \left. + \phi_{\text{opt}}^b + \phi^b] + \frac{\beta}{2} \cos[(\omega_{\text{opt}} - \omega_{\text{RF}})t + \phi_{\text{opt}}^b - \phi^b] \right]
 \end{aligned} \tag{1}$$

where  $\omega_{\text{opt}}t + \phi_{\text{opt}}^a$  and  $\omega_{\text{opt}}t + \phi_{\text{opt}}^b$  are the phases of the optical carriers at the modulators, and the constants  $\alpha$  and  $\beta$  are determined by the conversion efficiency and modulation depth respectively. The first term in the expansions of  $E^a$  and  $E^b$  represents the carrier component which contains no information about the millimeter-wave signal. The second and third terms, which represent the upper and lower sidebands (USB and LSB), contain the required signal information. Assuming that the phase of the local oscillators can be controlled such that  $\phi_{\text{opt}}^a = \phi_{\text{opt}}^b$  (which can be achieved using

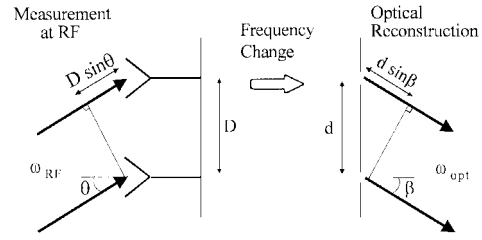


Fig. 2. Optical reconstruction of a RF point source.

the phase calibration techniques described later) it can be seen that the phase differences between the optical signals in the upper ( $\Delta\phi_{\text{opt}}^+$ ) and lower ( $\Delta\phi_{\text{opt}}^-$ ) sidebands are

$$\begin{aligned}
 \Delta\phi_{\text{opt}}^+ &= \phi^b - \phi^a = \Delta\phi_{\text{RF}} \\
 \Delta\phi_{\text{opt}}^- &= -(\phi^b - \phi^a) = -\Delta\phi_{\text{RF}}
 \end{aligned} \tag{2}$$

The modulation process does therefore preserve the information required to form an image, although in the lower sideband the phase difference is reversed in sign.

The process of image formation can be conceptually understood by considering the two antennas and a point source, as shown schematically in Fig. 2. The wavefront from a distant point source at an angle  $\theta$  to the optic axis arrives at the two antennas at different times, introducing a phase difference,  $\Delta\phi_{\text{RF}}$ , between the signals at the antennas given by

$$\Delta\phi_{\text{RF}} = \frac{\omega_{\text{RF}} D \sin \theta}{c} \tag{3}$$

where  $D$  is the antenna separation. The radiation is then heterodyned to the optical frequency ( $\omega_{\text{opt}}$ ) and emitted in the optical domain to form an interference pattern of sinusoidal fringes (Young's fringes), the spatial phase of which depends on the phase difference between the signals at the two apertures. As shown earlier, the RF phase difference between the receiving antennas on the input side,  $\Delta\phi_{\text{RF}}$ , is carried through to a phase difference of  $\Delta\phi_{\text{RF}}$  on the optical fringes and the point source leads to constructive interference at output angles ( $\beta$ ) given by

$$\sin \beta = \pm \left( \frac{\omega_{\text{RF}} D}{\omega_{\text{opt}} d} \sin \theta + m \frac{c}{\omega_{\text{opt}} d} \right) \tag{4}$$

where  $m$  is an integer, and the preceding  $+$  and  $-$  refer to the USB( $+$ ) and LSB( $-$ ), respectively. Each intensity peak of the fringes where constructive interference takes place, corresponds to a position of an "image" of the source through this two-aperture system.

For a single millimeter-wave frequency we can choose to set the term  $\omega_{\text{RF}} D / \omega_{\text{opt}} d$  in (4) equal to unity, meaning that the aperture separations are scaled by the ratio of the millimeter-wave and optical frequencies. In this case, a bright fringe corresponding to the image of the source is formed at  $\beta = \theta$  (for  $m = 0$ ). If the source moves through an angle  $\Delta\theta$  then this image moves through the same angle and it is clear that an extended source would be imaged with good fidelity. If for practical considerations we choose to set  $\omega_{\text{RF}} D / \omega_{\text{opt}} d$  to a value other than unity the input and output angles are scaled by this factor, giving a magnified or demagnified image. In

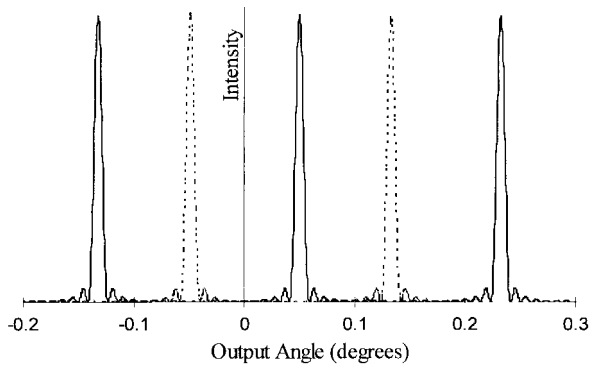


Fig. 3. Optical image intensity with a single monochromatic point source (RF frequency 94 GHz, optical wavelength  $1 \mu\text{m}$ , antenna element spacing 1 m, fiber element spacing  $314 \mu\text{m}$ ,  $\theta = 0.05^\circ$ ). Solid Line: USB, Dotted Line: LSB.

practice, more than two antennas will be required to generate a satisfactory point spread function for the instrument. The above arguments hold for a multielement array provided that the geometry of the 2-D optical array matches that of the millimeter-wave array.

As an example, Fig. 3 shows the simulated image intensity using a one-dimensional (1-D) array with 20 equally spaced antennas and a single monochromatic point source located at an input angle of  $0.05^\circ$ . Because the millimeter-wave and optical array dimensions have been scaled by the ratio of the millimeter-wave and optical frequencies, the system has a magnification of unity and the solid line shows an image of the point source at  $0.05^\circ$  ( $m = 0$ ), arising from the USB. The other two peaks correspond to grating responses of the array which would, in practice, be minimized by careful array design and attenuated by the envelope of a single dish (not included in simulation). The dotted line in Fig. 3 shows the image formed by the LSB which, because the phase relationship is  $\Delta\phi_{\text{opt}}^- = -\Delta\phi_{\text{RF}}$ , has a peak at  $-0.05^\circ$  ( $m = 0$ ). The carrier frequency [first term in the expansion of (1)] would also produce a fringe centred on the origin (not shown in Fig. 3). To avoid confusion between positive and negative bearings and to produce a usable image these extra images must be suppressed. Thus, one of the major conclusions of this analysis is that one sideband and the carrier frequency must be filtered out, hence a single sideband suppressed carrier modulation scheme must be used. Such modulators, fabricated in integrated optics, have been demonstrated for optical communications applications, where they offer advantages such as spectral and power efficiency and reduction in optical dispersion properties [16], [17] Their use in the telecommunications industry is likely to increase their availability and reduce their cost.

Although the experiments described later in this paper were performed with a narrowband RF, it is instructive to consider the effect of using a finite RF bandwidth, which in any real system would be necessary in order to achieve a satisfactory sensitivity. The term  $\omega_{\text{RF}}D/\omega_{\text{opt}}d$  in (4) can be thought of as an effective angular magnification which, with a finite RF bandwidth, is frequency dependent. A point source at angle  $\theta$  will therefore be reconstructed at a different angle ( $\beta$ )

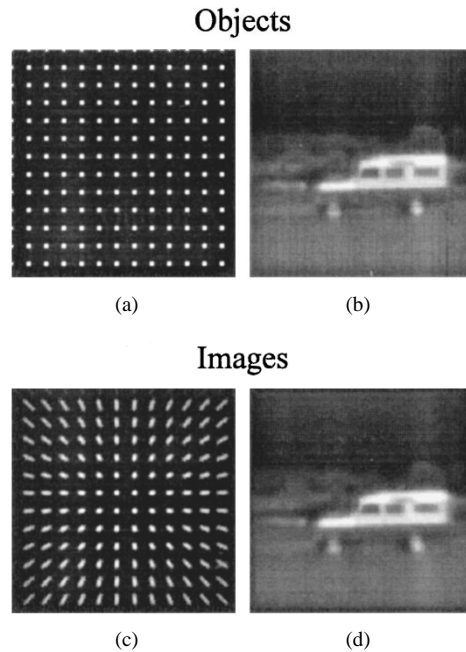


Fig. 4. Simulations of 2-D images demonstrating frequency dependent magnification (not through an array). (a) simulated test object, (b) real test object: millimeter-wave image of a Land Rover, and (c) and (d) effect of frequency dependent magnification with a 10% RF bandpass.

for every RF frequency, resulting in blurring in the image, to a degree determined by the fractional bandwidth of the RF signal and the off-axis angle of the source ( $\theta$ ). The optimum IF bandwidth for low noise temperature millimeter-wave radiometers is however about only 2 GHz, giving a fractional bandwidth that for single sideband detection is only 2% and for double sideband is unlikely to be greater than 8%. The effect of the frequency-dependent magnification in this case is illustrated in Fig. 4 in which *a* and *b* are test objects and *c* and *d* demonstrate the degree of blurring with a 10% RF bandwidth (which leads to a blurring of 5% of the full angular field of view at the extremes of the image). The images illustrate the increase in blurring with angle off boresight and indicate that this level of blurring may be perfectly acceptable, depending on the content of the scene. These are not simulations of imaging through an array, but illustrate the level of blurring on a filled aperture image.

### III. PHASE CONTROL

#### A. Origin of Phase Errors

In any aperture synthesis instrument care must be taken to control the signal phase in the paths from each antenna to an accuracy of less than one tenth of a wavelength in order to achieve high quality images. In a millimeter-wave instrument phase errors are likely to be introduced by errors in positioning of individual antennas, phase errors in the local oscillator (RF or laser) and variations in path lengths from the antennas to the image plane. All of these sources of error are likely to require real-time phase calibration. In the coherent optical beam-forming system described here, interference of

the laser light itself is used to form the image, hence the fiber paths from each antenna must be controlled to less than a tenth of the optical wavelength ( $\sim 0.1 \mu\text{m}$ ). These fiber paths are sensitive to both temperature and strain, hence an active phase control system will be necessary and the issue of phase calibration is important in assessing the practicality of the proposed system.

One approach to phase control is to calibrate each part of the system independently, for example using absolute calibration of fiber path lengths and the use of shape sensors to measure the antenna positions. Such calibration of fiber path lengths to the required accuracy has been demonstrated in optical fiber interferometry [18]. An alternative approach is to perform a single phase calibration procedure that eliminates all of the sources of phase error listed above in one step. The technique used, called redundant spacings calibration (RSC), allows real-time, model-independent phase calibration and may be applied at any wavelength [19], [20]. RSC has been demonstrated recently at millimeter and optical wavelengths, and has been shown to operate down to signal-to-noise ratios (SNR's) of approximately 3 [21]. It is also proposed for calibration of MIRAS, the future ESA L-band remote sensing aperture synthesis radiometer [22]. In this paper it is applied to the phase calibration of a coherent optical beam-forming system for the first time.

### B. Redundant Spacings Calibration

An array of  $N$  antennas provides  $N(N-1)/2$  collector pairs or baselines, each of which measures a particular spatial frequency of the source brightness distribution and which may be corrupted by phase errors at each element in the array. The RSC approach relies on the principle that if two pairs of antennas have the same vector spacing then each pair measures the same Fourier component of the scene. If these two measured values differ then that difference can only be due to instrumental or atmospherically induced aberrations. This provides a mechanism by means of which such phase errors can be distinguished from the characteristics of the scene without the need for model-building, or other a priori assumptions about the scene, except that it consists of spatially incoherent radiation and is in the observer's far field.

The measured phase of the mutual coherence function  $m_{ij}$  over a baseline containing antennas labeled  $i$  and  $j$  is given by

$$m_{ij} = \phi_{ij} + e_i - e_j \quad (5)$$

where  $\phi_{ij}$  is the true phase and  $e_i$  and  $e_j$  are the individual antenna phase errors. For an  $N$ -element array we can write  $N(N-1)/2$  equations of this type but there is not enough information to distinguish the true phases from the phase errors. In order to perform self-calibration the array must be designed with at least  $N-3$  redundant baselines, leading to equations of the type  $\phi_{ij} = \phi_{kl}$ , and three disposable parameters of the type  $e_i = 0$  or  $\phi_{ij} = 0$ . All of these equations can be combined in matrix form as

$$M = AU \quad (6)$$

where the vector  $M$  contains the measured baseline phases ( $m_{ij}$ ),  $U$  contains the unknown baseline phases ( $\phi_{ij}$ ) and

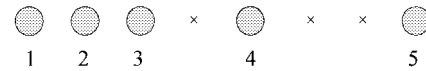


Fig. 5. The RSC array design used in the experiments.

phase errors ( $e_i$ ) and  $A$  includes information about the redundant baselines and disposable parameters. The corrected baseline phases are then obtained by inverting matrix  $A$  to give the antenna phase errors from

$$U = A^\dagger M. \quad (7)$$

The pseudo-inverse matrix  $A^\dagger$  depends only on the array design and can be precomputed making phase correction very fast and potentially real-time.

### C. CCD-Based RSC

The RSC technique relies on the availability of phase measurements ( $m_{ij}$ ) over each baseline in the array. In general these can be obtained by measuring the position of the fringe pattern from each pair of apertures, in the image plane. However, the redundant baselines, necessary for phase calibration, generate fringes with the same period and orientation. The RSC data processing scheme requires that these two fringe systems are measured independently. This can be achieved by measuring two images with and without phase shifts of  $\pi$  radians added to particular apertures. We have developed a technique using simple optics, a diffraction grating and a single CCD to measure the two images simultaneously [21]. This allows all of the baseline phases to be extracted in a single snapshot, which is advantageous when phase errors are changing rapidly. In order to achieve the required phase shifts the grating is translated by a quarter of a period over one, and only one, of the collectors involved in each redundant measurement.

If an amplitude grating is used three images are recorded on the CCD, corresponding to the zero, +1 and -1 diffraction orders. The zero-order image is the image that would have been obtained directly through the array, including all aberrations, whereas the images in the +1 and -1 orders are affected by the grating shifts. All fringes formed from baselines in which the grating behind just one aperture of the pair has been displaced are shifted by half a fringe period between the +1 and -1 order images. Addition and subtraction of these two orders allows separation of the fringe patterns from redundant baselines and extraction of the phases is possible. The zero-order image is not used for image reconstruction.

## IV. EXPERIMENTS

A proof of principle experiment has been performed to demonstrate coherent optical beam forming with a single point source and real-time calibration of phase errors. For convenience a linear antenna/fiber array was used and no attempt was made to examine the blurring effect of broad-band operation, with all measurements being made narrowband at a frequency of 2 GHz. The modulation scheme was simple double sideband without suppression of the carrier, hence

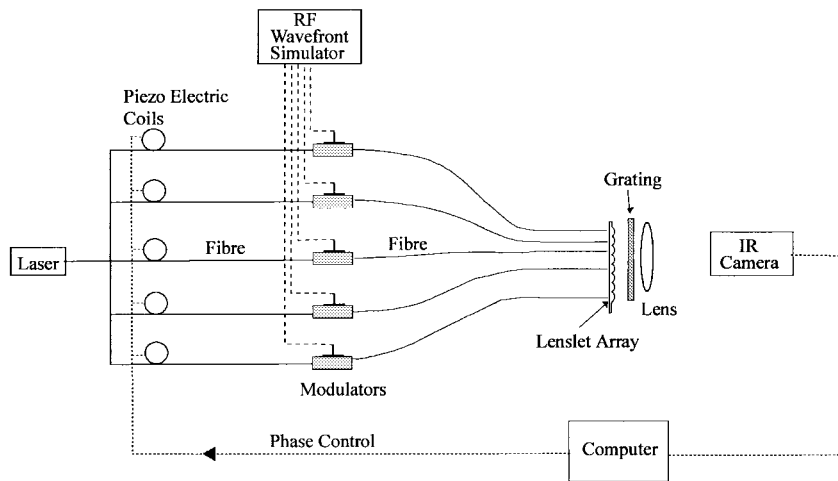


Fig. 6. A schematic diagram of the experimental system.

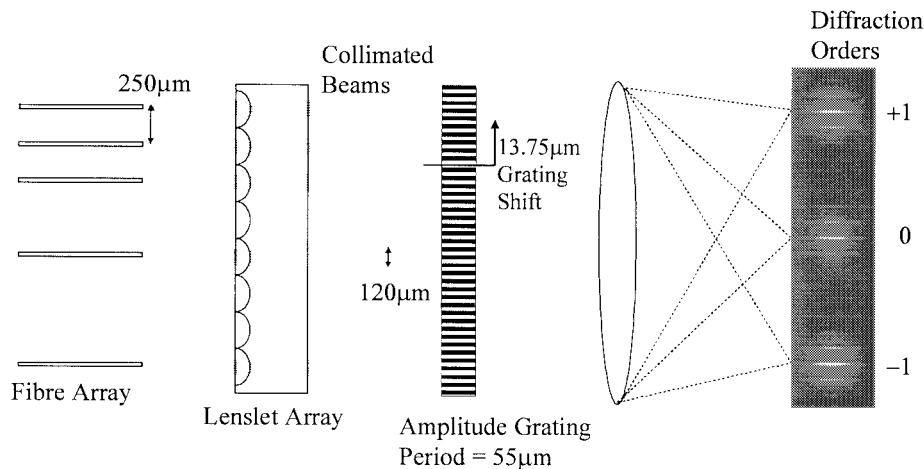


Fig. 7. An expansion of the optical side of the experimental system.

the image contained a boresight component due to the non-suppressed laser frequency (even in the absence of any RF signal) and two images of the source corresponding to the two sidebands when the RF was applied. Although this was nonoptimum it did not prevent observation of the optical image of the RF source.

Real-time calibration of phase errors (introduced largely by time-dependent temperature fluctuations in the optical fibers) was achieved using RSC with a five-element linear array which had enough redundancy built in to allow self-calibration. The array, shown in Fig. 5, is based on an eight-element equally spaced array with three of the elements removed. This allowed RSC to be implemented using the grating technique described above, with the grating shifted by quarter of a period over apertures 1 and 2.

The experimental setup is shown in Fig. 6. The laser, a diode pumped ND:YAG (10 mW @ 1300 nm), is split into five optical fibers which transmit the light to electrooptic amplitude modulators (lithium niobate: 0–2.5 GHz). Each fiber contains a phase controller consisting of a piezoelectric drum which is used to apply phase corrections to each arm of the system under computer control (1 V gives  $\sim\pi$  radians phase

shift). The RF signal applied to each modulator was generated by a wavefront simulator which generated five channels of monochromatic RF signal, each with adjustable phase to allow simulation of an off-axis point source. The optical outputs from the modulators travel through fiber to the imaging end of the system where the fibers are glued into a precision machined silicon “V” groove (250  $\mu\text{m}$  spacing) to form the five-element array shown in Fig. 5. Light from the fibers is collimated using a lenslet array with a 650  $\mu\text{m}$  focal length (Fig. 7), giving a beam diameter of approximately 120  $\mu\text{m}$ . The light then passes through a 55- $\mu\text{m}$  period amplitude diffraction grating, which is shifted by 13.75  $\mu\text{m}$  over apertures 1 and 2, and a lens which forms the image onto an infrared camera. The grating shift allows extraction of all of the phase information required for RSC phase control.

The image on the camera consists of the zero, plus one and minus one diffraction orders (Fig. 7). The +1 ( $J_1$ ) and -1 ( $J_2$ ) order images were extracted from each snapshot image and the required baseline phases ( $m_{i,j}$ ) calculated from the Fourier transforms of  $J_1 + J_2$  and  $J_1 - J_2$ . The phase errors relating to each fiber arm were then calculated from (7), which

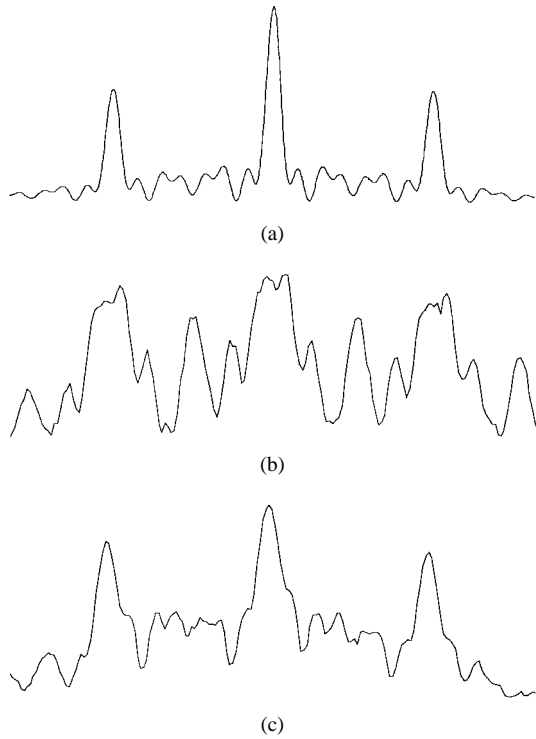


Fig. 8. Cross-sections through the zero order diffraction pattern. (a) Simulated with no optical phase errors, (b) measured without RSC running, and (c) measured with RSC running.

for this array takes the form

$$\begin{bmatrix} e_1 \\ e_2 \\ e_3 \\ e_4 \\ e_5 \end{bmatrix} = \begin{bmatrix} 0 & 0 & 0 & 1 & 0 \\ 0 & 0 & 0 & 1 & -1 \\ 1 & 0 & 0 & 1 & -2 \\ 2 & 1 & 0 & 1 & -4 \\ 4 & 2 & 1 & 1 & -7 \end{bmatrix} \begin{bmatrix} m_{12} - m_{23} \\ m_{13} - m_{34} \\ m_{24} - m_{45} \\ 0 \\ m_{12} \end{bmatrix} \quad (8)$$

where the phase error on fiber 1 ( $e_1$ ) and the object phase ( $\phi_{12}$ ) have been set to zero. The calculated phase errors were then applied as corrections to each fiber using the fiber piezocoils.

With no RF signal, only the diffraction pattern due to the carrier signal was detected on the camera. The theoretical perfect point spread function of the array, shown in Fig. 8(a), has a large central peak and two grating responses. The relatively high sidelobes are due to the small number of antennas used in this experiment and would be reduced in any practical system by more careful array design. With the phase control loop inactive the diffraction pattern was very unstable, varying at frequencies of greater than 1 Hz due to thermal drifts in the optical fibers. Fig. 8(b) shows the cross-section through a typical uncorrected image (zero order). When the control loop (with a bandwidth of at  $\sim 13$  Hz) was activated the image stabilised resulting in the image shown in Fig. 8(c). The improvement in image quality, from a time-varying aberrated image to a stable corrected image with the 3 distinct peaks of the ideal image, was very dramatic when seen in the laboratory. The differences between Fig. 8(a) and Fig. 8(c) are due mainly to experimental difficulties, in particular the infrared camera used which had a slow time response and nonuniformities which produced an overall hump in the image which can clearly be seen in Fig. 8(c). These

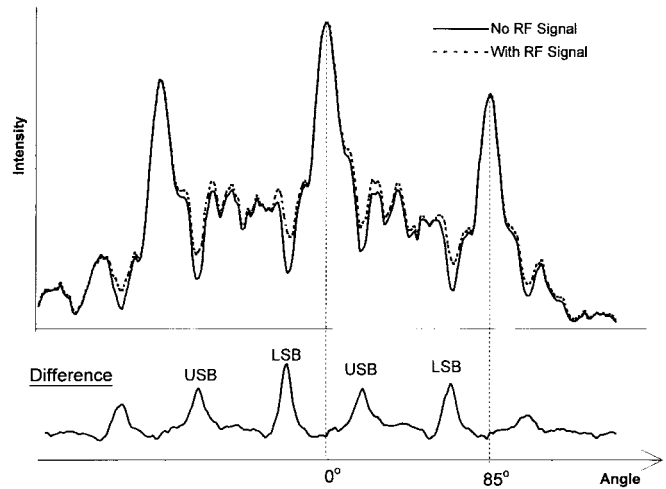


Fig. 9. Optical image of an off-axis RF point source. Upper graph shows measurements of the optical diffraction pattern with and without an applied RF signal. Lower plot shows the difference between these two plots, representing the optical image of the RF point source (USB/LSB refer to upper/lower optical sidebands).

images do however demonstrate the use of RSC for real-time phase calibration and control.

The RF simulator was then used to apply a simulated wavefront to the five modulators. The solid line in Fig. 9 shows the experimentally measured optical intensity with no RF signal and the dotted line shows the optical intensity when a RF signal was applied, simulating a point source  $22^\circ$  off-axis. The difference between these two curves (lower plot in Fig. 9) shows an "image" of the RF point source at  $22^\circ$  in the upper sideband. The multiple peaks are due to the presence of both the upper and lower sidebands and appear at the predicted locations. As the source angle was varied the image peaks moved across the camera in a predictable way, showing that the system would be capable of generating the image of an extended scene.

These proof of principle experimental results confirm the theoretical prediction that the upper and lower sidebands produce images of a point source at angles of equal magnitude but opposite sign. They also emphasise the need for suppression of the optical carrier frequency to enable imaging close to boresight and to allow the full dynamic range of the camera to be used to record the signal of interest.

## V. CONCLUSION

An all-optical signal transport and image formation technique has been described for use with a 2-D passive millimeter-wave aperture synthesis array. The technique offers significantly less complexity than an instrument making discrete correlation measurements over each baseline in the array. In a system with  $N$  antennas, the major components in the beamforming network described in this paper are the  $N$  optical modulators, compared to the  $N \times (N-1)$  way splitters and  $N(N-1)/2$  complex correlators required in the alternative system. The direct optical image, that can be detected with a standard CCD camera, is also an advantage. The approach also offers greater bandwidth and hence sensitivity than a

previously reported optical processing technique which used frequency scanned antennas [15].

A proof of principle experiment has demonstrated the ability to form a direct optical image of a RF point source using a nonoptimized array. It has been shown that phase calibration of the optical fibers, to eliminate phase errors due to thermal drift, can be achieved through self-calibration using redundant spacings calibration. The theory and experimental results emphasise the need for removal of the optical carrier frequency to increase the dynamic range and use of a single sideband only to remove directional ambiguity. Single sideband suppressed carrier modulators have already been developed and demonstrated and their cost is likely to be driven down by telecommunications and radar requirements. As such modulators become widely available, the proposed system will offer an attractive and potentially low cost route to implementing a passive millimeter-wave array-based imager.

#### REFERENCES

- [1] R. Appleby and A. H. Lettington, "Passive millimeter wave imaging," *Electron. Commun. Eng. J.*, vol. 3, pp. 13–16, 1991.
- [2] R. Appleby, D. G. Gleed, R. N. Anderton, and A. H. Lettington, "High performance passive millimeter-wave imaging," *Optic. Eng.*, vol. 32, pp. 1370–1373, 1993.
- [3] A. R. Thompson, J. M. Moran, and G. W. Swenson, *Interferometry and Synthesis in Radio Astronomy*. New York: Wiley, 1986, pp. 40–56.
- [4] L. Xu, R. Taylor, and S. R. Forrest, "The use of optically coherent detection techniques for true-time delay phased array and systems," *J. Lightwave Technol.*, vol. 13, pp. 1663–1678, Aug. 1995.
- [5] R. Benjamin and A. J. Seeds, "Optical beamforming techniques for phased array antennas," *Inst. Elec. Eng. Proc.—H*, 1992, vol. 139, pp. 526–534.
- [6] K. Yamada, I. Chiba, and Y. Karasawa, "Frequency characteristics of a beamforming network of an optically controlled array antenna and its radiation pattern measurements," *IEICE Trans. Electron.*, vol. E79-C, no. 1, pp. 68–73, 1996.
- [7] Y. Ji, K. Inagaki, R. Miura, and Y. Karasawa, "Optical processor for multibeam microwave array antennas," *Electron. Lett.*, vol. 32, no. 9, pp. 822–824, 1996.
- [8] G. A. Koepf, "Optical processor for phased-array antenna beam formation," *Optic. Technol. Microwave Applications*, SPIE, vol. 477, pp. 75–81, 1984.
- [9] L. P. Anderson, F. Boldissar, and D. C. D. Chang, "Antenna beamforming using optical processing," *Optoelectron. Signal Processing for Phased-Array Antennas*, SPIE, vol. 866, pp. 228–232, 1988.
- [10] D. Dolfi, F. Michel-Gabriel, S. Bann, and J. P. Huignard, "Two-dimensional optical architecture for time-delay beam forming in a phased-array system," *Opt. Lett.*, vol. 16, no. 4, pp. 255–257, 1991.
- [11] K. P. Jackson, S. A. Newton, B. Moslehi, M. Tur, and C. Cutler, "Optical fiber delay-line signal processing," *Inst. Elec. Eng. Trans. Microwave Theory Tech.*, vol. MTT-33, pp. 193–210, 1985.
- [12] R. D. Esman, M. Y. Frankel, J. L. Dexter, L. Goldberg, M. G. Parent, D. Stilwell, and D. G. Cooper, "Fiber-optic prism true time-delay antenna feed," *IEEE Photon. Technol. Lett.*, vol. 5, pp. 1347–1349, Nov. 1993.
- [13] A. Molony, L. Zhang, J. A. R. Williams, I. Bennion, C. Edge, and J. Fells, "Fiber Bragg grating time delay control of phased array antenna," *J. Mod. Opt.*, vol. 43, pp. 1017–1024, 1996.
- [14] A. C. Young, "Optical fibers in radio astronomy," in *Proc. IAU: Very High Angular Resolution Imaging*, G. Robertson, W. J. Tango, Eds. London, England: Kluwer Academic, 1994, pp. 227–234.
- [15] J. Lovberg, R. C. Chou, and C. Martin, "Real-time millimeter-wave imaging radiometer for avionic synthetic vision," *SPIE*, vol. 2220, pp. 234–244, 1994.
- [16] F. Heismann and R. Ulrich, "Integrated-optical single-sideband modulator and phase shifter," *IEEE J. Quantum Electron.*, vol. QE-18, pp. 767–771, Apr. 1982.
- [17] M. Y. Frankel and R. D. Esman, "Optical single-sideband suppressed-carrier modulator for wide-band signal processing," *J. Lightwave Technol.*, vol. 16, pp. 859–863, May 1998.
- [18] D. A. Flavin, R. Mc Bride, J. D. C. Jones, J. G. Burnett, and A. H. Greenaway, "Combined temperature and strain measurement with a dispersive optical fiber Fourier-transform spectrometer," *Opt. Lett.*, vol. 19, pp. 2167–2169, 1994.
- [19] A. H. Greenaway, "Prospects for alternative approaches to adaptive optics," in *Adaptive optics for Astronomy*, D. M. Alloin, J.-M. Mariotti, Eds. NATO ASI Series C. 423, 1994.
- [20] ———, "Self-calibrating dilute-aperture optics," *SPIE*, vol. 1351, pp. 738–748, 1990.
- [21] P. M. Blanchard, A. H. Greenaway, R. A. Anderton, and R. Appleby, "Phase calibration of arrays at optical and millimeter wavelengths," *J. Opt. Soc. Amer. A.*, vol. 13, pp. 1593–1600, 1996.
- [22] M. Martin-Neira, J. M. Goutoule, A. Knight, J. Claude, J. Bara, A. Camps, F. Torres, I. Corbella, A. Lannes, E. Anterrieu, B. Laursen, and N. Skou, "Integration of MIRAS breadboard and future activities," in *Proc. IEEE Geosci. Remote Sensing Symp.*, 1996, pp. 869–871.

**P. M. Blanchard**, photograph and biography not available at the time of publication.

**A. H. Greenaway**, photograph and biography not available at the time of publication.

**A. R. Harvey**, photograph and biography not available at the time of publication.

**K. Webster**, photograph and biography not available at the time of publication.